Combination of Supervised and Unsupervised Methods for Navigation Path Mining

Naoya Ohnishi, Atsushi Imiya

Combination of Supervised and Unsupervised Methods for Navigation Path Mining

Naoya Ohnishi[1] ** and Atsushi Imiya[2]

[1] School of Science and Technology, Chiba University, Japan
Yayoicho 1-33, Inage-ku, Chiba, 263-8522, Japan
[2] Institute of Media and Information Technology, Chiba University, Japan
Yayoicho 1-33, Inage-ku, Chiba, 263-8522, Japan
imiya@faculty.chiba-u.jp

Abstract. In this paper, we introduce a statistical learning method for the visual navigation of the mobile robot. For the visual navigation of an autonomous robot, the detection of the collision avoidance navigation direction from an image/image sequence captured by imaging systems mounted on the robot is a fundamental task. The robot detects the free space for the navigation and computes the collision-free direction. For the extraction of the free space, the robot separates the dominant plane and obstacle area using independent component analysis. For the computation of the collision avoidance direction, our robot computes the principal component of the gradient of the visual potential field which describes the obstacle area. Some experimental results of navigating the mobile robot in synthetic and real environments are presented.

1 Introduction

For the visual control of an autonomous robot, the detection of the collision-avoidance navigation direction from an image/image sequence is a fundamental task. The robot mounting with a monocular and/or multiple vision system computes the control features from the view in front of the robot. In this paper, we introduce a combination of supervised and unsupervised methods for the visual navigation of an autonomous mobile robot. Figure 1 illustrates the relation between the collision-avoidance direction and the visual navigation strategy. Since the view of the space without any obstacles is an ideal supervisor for the free space detection, we use supervised method for the free space detection. To allow the robot to navigate without any maps, we use unsupervised method to decide the navigation direction. For the detection of the free space, we use independent component analysis of the optical flow field captured by the imaging system on the robot [15], and for the determination of the navigation direction, we use principal component analysis of the visual potential field [13].

** Present Address: Power and Industry Systems Research and Development Centers, Power Systems Company, TOSHIBA, Fuchu, Tokyo, Japan.

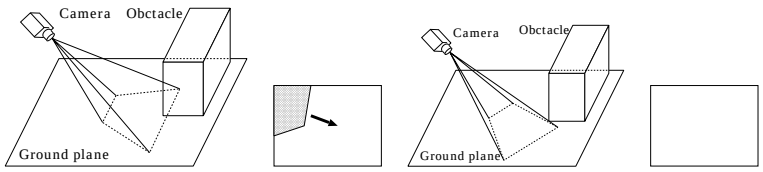

Fig. 1. Visual navigation strategy. (a) Distribution of obstacle and camera at time t. (b) Captured image at time t. The black region represents the obstacle. The arrow is the direction to the next view. (c) Distribution of the obstacle and camera at time $t+1$. (d) Captured image at time $t+1$. The distribution of obstacle areas on the image at t defines the direction to the next view at the time $t+1$, so that, at the time $t+1$, no obstacle is captured by the camera system mounted on the robot.

Independent component analysis (ICA) [5] extracts statistically independent features from signals for magnetoencephalography and and steal images for texture analysis. The optical flow field observed by a moving vision system can be assumed to be a mixture of patterns in an environment [15]. In cognitive neuroscience, it is known that the medial superior temporal (MST) area performs visual motion processing. For motion cognition at the MST area in the field 7a of the brain [16, 19], it is shown that independent components of optical flow are used. Therefore, ICA allows us to separate the blind source signals of optical flow into independent components. Furthermore, since the optical flow field on an image can be represented as a linear combination of independent components of optical flow[16], we can use ICA to detect a ground plane by separating obstacles and a dominant part in an image. Statistical approaches to the optical flow analysis have also been examined [4, 17]. Fermüller et al. analysed noise parameters of optical flow using the maximum likelihood [4]. Roth and Black developed a method for learning the spatial statistics of optical flow fields using a Markov random field model [17]. Therefore, it is appropriate to use the statistical properties of optical flow for mobile robot navigation in a real environment.

The potential field method [10] is an established method of path planning for mobile robots. Mobile robot navigation by the potential field method using a monocular or stereo camera has also been proposed [1, 11, 18]. Adorini et al. [1] used calibrated omnidirectional cameras for obstacle detection. Murray and Little [11] proposed an algorithm for the autonomous exploration by a mobile robot using calibrated stereo vision. Wong and Spetsakis [18] used optical flow observed through a calibrated monocular camera. Path planning is the problem of deriving the optimal or suboptimal path from a starting point to a destination using the map of the robot workspace, which is called the configuration space, and landmarks [7].

The robot navigation is achieved by computing the optimal navigation direction from a sequence of snapshots of the obstacle configuration in the robot

workspace [3]. Our method decides the navigation direction using the visual potential field and optical flow field of the image. The optical flow field [8] is an apparent motion of points on the imaging plane and a fundamental feature for understanding the motions of objects in the workspace for the robot. Since both the visual potential field and optical flow field provide apparent information on the image captured by the camera mounted on the mobile robot, our method does not require environmental maps or camera calibration for the robot navigation.

The visual potential is the summation of the gradient field in the obstacle area and the optical-flow field [13]. In this paper, we use the principal component of the gradient field as the control force. For the visual navigation, the robot computes the attractive force from the obstacle area to the feasible region to avoid colliding with obstacles in the workspace. Using this attractive force to avoid colliding with the obstacles, our robot adopts the principal direction of the gradient field computed using the obstacle region in the image. Therefore, our robot uses the principal direction of the gradient field and the optical flow as the attractive force from the obstacle and the guiding force to the destination, respectively.

2 Classification of Space using ICA

Optical Flow and Dominant Plane We define the dominant plane as a planar area in the workspace corresponding to the largest part in an image. The dominant planar part in an image is called the dominant plane [12]. We adopt the assumptions in ref. [15] for the robot navigation.

1. The ground plane, on which the robot moves, is the planar area.
2. The camera mounted on the mobile robot is downward-pointing.
3. The robot observes the world using the camera mounted on itself for navigation.
4. The camera on the robot automatically captures a sequence of images since the robot is moving.

The robot does not touch the obstacles. Therefore, if there are no obstacles around the robot, the ground plane corresponds to the dominant plane in the image observed through the camera mounted on the mobile robot. Using the sequence of optical flow field computed by the image sequence captured by the imaging system mounted on the robot, it is possible to extract the free space for the robot navigation.

Setting $I(x, y, t)$ and $\boldsymbol{u} = (u, v)^\top = (\dot{x}, \dot{y})^\top$ to be the time-varying gray-scale-valued image at time t and the optical flow vector, respectively, the optical flow vector $\dot{\boldsymbol{x}}$ at each point $\boldsymbol{x}$ satisfies $I_x u + I_y v + I_t = 0$. We use the Lucas-Kanade method with pyramids [2]. Using the pyramid transform, the optical flow field is computed using the following algorithm, where u and w stand for the optical flow computational algorithm at each pyramid level and the warping operation, respectively, and where $w(I, \dot{\boldsymbol{x}}) = I(\boldsymbol{x} + \dot{\boldsymbol{x}})$. In the algorithm, $\dot{\boldsymbol{x}}_t^l = (\dot{x}^l, \dot{y}^l)^\top$ is

computed from $\dot{\boldsymbol{x}}_t^{l+1} = (\dot{x}^{l+1}, \dot{y}^{l+1})^\top$ as $\dot{x}^l = E(\dot{x}^{l+1})$ and $\dot{y}^l = E(\dot{y}^{l+1})$, where the operation E expresses the upsampling to yield the optical flow field in the l-th layer from that in the $(l+1)$-th layer. In this algorithm, I_t^l stands for the pyramidal representation at level l of image $I(x, y, t)$ at time t.

Algorithm 1: Optical Flow Computation by the Lucas-Kanade Method Using Pyramids

Data: I_t^l, I_{t+1}^l, $\quad 0 \leq l \leq$ the maximum of the layers;
Result: $\dot{\boldsymbol{x}}^l$;
$l :=$ the maximum of the layers ;
while $l \neq 0$, **do**
  $\dot{\boldsymbol{x}}^l := u(I_t^l, I_{t+1}^l)$;
  $I_{t+1}^{l-1} := w(I_{t+1}^{l-1}, \dot{\boldsymbol{x}}_t^l)$;
  $l := l - 1$;
end

Assuming that the camera displacement is small, the corresponding points $\boldsymbol{x} = (x, y)^\top$ and $\boldsymbol{x}' = (x', y')^\top$ on the dominant planes between a pair of successive two images are connected with an affine transform, so that, $\boldsymbol{x}' = \boldsymbol{A}\boldsymbol{x} + \boldsymbol{b}$, where $\boldsymbol{A}$ and $\boldsymbol{b}$ are a 2×2 affine-coefficient matrix and a 2-dimensional vector, respectively. Using this affine transform, we can estimate the optical flow vector on the dominant plane $\hat{\boldsymbol{x}} = (\hat{x}, \hat{y})^\top$, $\hat{\boldsymbol{x}} = \boldsymbol{x}' - \boldsymbol{x} = (\boldsymbol{A}\boldsymbol{x} + \boldsymbol{b}) - \boldsymbol{x}$, for all points in the image. It is possible to estimate the matrix $\boldsymbol{A}$ and the translation vector $\boldsymbol{b}$ using appropriate methods [12]. If an obstacle exists in front of the robot, the vector $\hat{\boldsymbol{x}}$ on the image plane differs from the optical flow on the image plane. Therefore, if we have the optical flow of the ground flow without any obstacles, we can discriminate the dominant plane and obstacle area using differences of the flow vectors in the optical flow field.

ICA of Optical Flow Field As previously introduced [16, 19], we accept the assumption that the optical flow fields observed by the moving camera are linear combinations of the optical flow fields of the dominant plane and the obstacles [15]. This assumption is numerically and geometrically acceptable if motion displacement is small compared with the size of obstacles, as shown in the numerical experiment. Therefore, ICA is suitable for the separation of the optical flow field into independent flow components. We use the algorithm proposed in ref. [15].

ICA requires at least two input signals for separation of an input signal into two independent components. For the supervisor signal to ICA, we first prepare the optical flow vectors from of the model image $\hat{I}(x, y, t)$ without any obstacles. After computing of the optical flow $\hat{\boldsymbol{u}}(t)$ of the model image $\hat{I}(x, y, t)$ for the frames $t = 0 \ldots n$, the supervisor signal $\hat{\boldsymbol{u}}$ is computed as the average,

$$\hat{\boldsymbol{u}} = \frac{1}{n} \sum_{t=0}^{n} \hat{\boldsymbol{u}}(t). \tag{1}$$

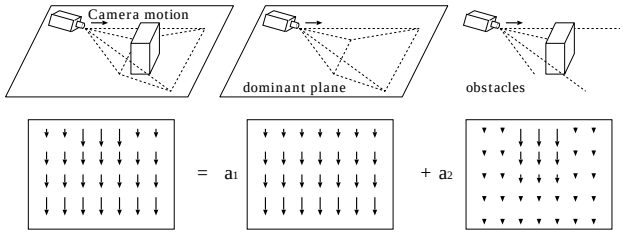

Fig. 2. Linear combination of optical flow field in the scene. The optical flow field (bottom right) is expressed as a linear combination of those shown at bottom middle and bottom right. a_1 and a_2 are mixture coefficients.

We use the optical flow field $\boldsymbol{u}$ and planar flow field $\hat{\boldsymbol{u}}$ for the inputs to ICA. The planar flow is the motion of the dominant plane relative to the robot motion.

Setting $\boldsymbol{v}_\alpha$ and $\boldsymbol{v}_\beta$ to be the output optical flow fields of ICA, we have the equations

$$\begin{cases} \boldsymbol{u} = a_{11}\boldsymbol{v}_\alpha + a_{12}\boldsymbol{v}_\beta \\ \hat{\boldsymbol{u}} = a_{21}\boldsymbol{v}_\alpha + a_{22}\boldsymbol{v}_\beta \end{cases}, \tag{2}$$

where a_{ij} is the mixture coefficient. ICA estimates the independent optical flow fields $\boldsymbol{v}_\alpha$ and $\boldsymbol{v}_\beta$ from optical flow field $\boldsymbol{u}$ and planar flow field $\hat{\boldsymbol{u}}$. The motions of the dominant plane and obstacles in the images are different, and the dominant-plane motion is smooth on the images compared with the obstacle motion, as shown in Fig. 3. Consequently, the output signal of the obstacle motion has larger variance than the output signal of the dominant-plane motion. We are required to determine whether components have optical flow of the dominant plane or of obstacle areas. The difference in the variances of the norms of vectors $\boldsymbol{v}_\alpha$ and $\boldsymbol{v}_\beta$ enables us to order independent components [15]. Therefore, if the variances σ_α^2 and σ_β^2, of $|\boldsymbol{v}_\alpha|$ and $|\boldsymbol{v}_\beta|$, respectively satisfy the inequality $\sigma_\beta^2 > \sigma_\alpha^2$, we accept the output flow field $\boldsymbol{v}_\alpha$ as the the optical flow field on the dominant plane.

Since the planar flow field is subtracted from the optical flow field including the obstacle motion, the speed $|\boldsymbol{v}(\boldsymbol{x})|$ of the point $\boldsymbol{x}$ is constant on the dominant plane. However, the length of the flow vector $|\boldsymbol{v}(\boldsymbol{x})|$ is not constant, because of the form of Eq. (2). Then, we use the median value of $|\boldsymbol{v}(\boldsymbol{x})|$ for the detection of the dominant plane. Since the dominant plane occupies the largest domain in the image, we compute the distance between each $|\boldsymbol{v}(\boldsymbol{x})|$ and the median of the speed, as shown in Fig. 3. The area which has the median value of the component is detected as the dominant plane. Setting m to be the median value of the speed, we define the measure as $\varepsilon(x, y, t) = ||\boldsymbol{v}(\boldsymbol{x})| - m|$. We detect the area in which $\varepsilon(x, y, t) \approx 0$ as the dominant plane, that is, we set

$$\text{Dominant plane } D \text{ of the time } t \ = \{\boldsymbol{x} = (x, y)^\top | \varepsilon(x, y, t) \approx 0\}. \tag{3}$$

Definition 1. *(Dominant map) We call the function $d(x, y, t)$, which is zero in the dominant plane and one outside of the dominant plane, the dominant map.*

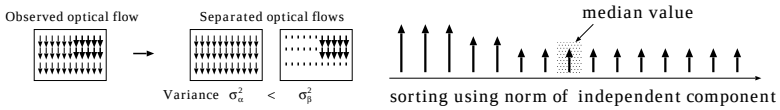

Fig. 3. Left: Difference in the motions of the dominant plane and obstacles. The dominant-plane motion is smooth on the images compared with obstacle motion. Therefore, the order of the components can be determined by using variances σ_α^2 and σ_β^2. Right: Sorting using the norm $\boldsymbol{l}$ for determination of output order. The area which has the median value of the component is detected as the dominant plane, since the dominant plane occupies the largest domain in the image.

Therefore, we have a two-phase algorithm for the separation of the free space for the navigation shown in Fig. 4

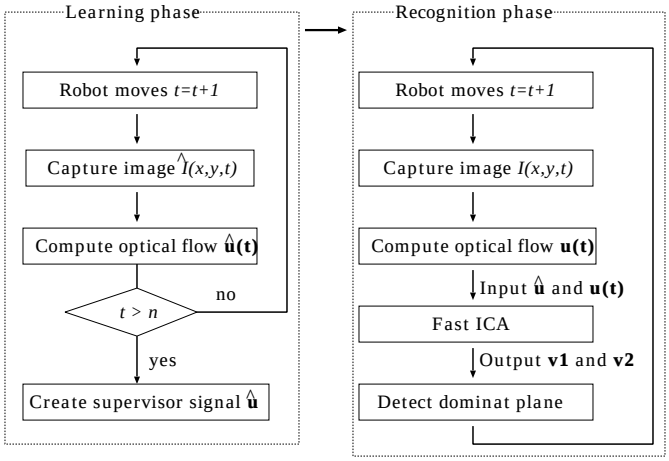

Fig. 4. Procedure for the free space detection using optical flow and ICA.

3 Visual Navigation using PCA

Gradient Vector of Dominant Plane as Repulsive Force Field For the navigation without colliding with obstacles, we generate an artificial repulsive force from the obstacle area in the dominant plane map $D(x, y, t)$ using the gradient vector field. The potential field on the image is an approximation of the projection of the potential field in the workspace to the image plane. Therefore, we use the gradient vector of the dominant plane as the repulsive force field from obstacles.

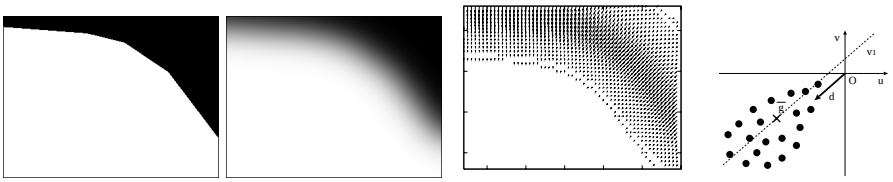

(a) $d(x,y,t)$ (b) $G*d(x,y,t)$ (c) $\boldsymbol{g}(x,y,t)$ (d)

Fig. 5. (a) Dominant plane map $d(x,y,t)$. The black and white regions indicate obstacle and dominant plane regions, respectively. (b) Dominant plane after Gaussian convolution operation $G*d(x,y,t)$. (c) Gradient vector field $\boldsymbol{g}(x,y,t)$ as repulsive force field from obstacles. Since the obstacle is at the upper right of the image, the directions of the gradient vectors are to the lower left. (d) Geometrical relationship between the principal component and the repulsive force. Black dots and x indicate the collection of gradient vectors $\mathbf{G} = \{\boldsymbol{g}_i\}_{i=1}^N$ and its mean value $\overline{\boldsymbol{g}}$, respectively. The dashed line and bold line indicate the principal component $\boldsymbol{v}_1$ and the repulsive force $\boldsymbol{r}$, respectively.

Definition 2. *(Obstacle region) We call the compliment of the dominant plane with respect to the imaging region the obstacle region O, that is, $O = \mathbf{R}^2 \setminus D$.*

Since the dominant plane map $d(x,y,t)$ is a binary image sequence, the computation of the gradient is numerically unstable and unrobust. Therefore, as a preprocess to the computation of the gradient, we smooth the dominant plane map $d(x,y,t)$ by convolution with Gaussian $G*$, that is, we adopt $\boldsymbol{g}$,

$$\boldsymbol{g}(x,y,t) = \nabla(G*d(x,y,t)) = \begin{pmatrix} \frac{\partial}{\partial x}(G*d(x,y,t)) \\ \frac{\partial}{\partial y}(G*d(x,y,t)) \end{pmatrix},$$

as the potential generated by obstacles. Here, for the 2D Gaussian, $G_\sigma(x,y) = \frac{1}{2\pi\sigma} e^{-\frac{x^2+y^2}{2\sigma^2}}$ we define

$$G*d(x,y,t) = \int_{-\infty}^{\infty}\int_{-\infty}^{\infty} G(u-x, v-y)d(x,y,t)dudv. \tag{4}$$

Definition 3. *(Obstacle potential) For the obstacle region O, we define the potential*

$$p_o(x,y,t) = G_\sigma * d(x,y,t) \quad d(x,y,t) = \begin{cases} 255, & \textit{if } \boldsymbol{x} \in O \\ 0, & \textit{otherwise,} \end{cases} \tag{5}$$

we define the gradient of the potential as

$$\boldsymbol{g}(x,y,t) = \nabla p_o(x,y,t). \tag{6}$$

We select the parameter σ to be half the image size. An example of the gradient vector field is shown in Fig. 5(c).

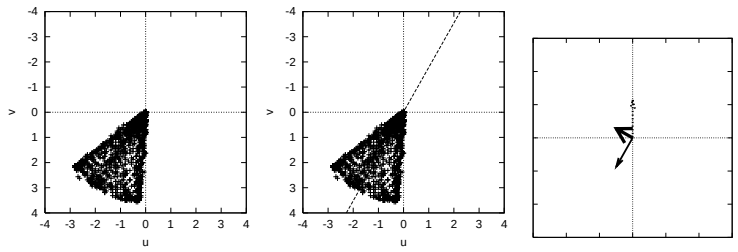

(a) $\mathbf{G}$ (b) $\boldsymbol{v}_1$ (c) $\boldsymbol{p}$

Fig. 6. Gradient field and its principal component. (a) $\mathbf{G} = \{\boldsymbol{g}_i\}_{i=1}^N$ of Fig. 5 is plotted in the u-v coordinate. (b) Plotted $\mathbf{G}$ and its first principal component $\boldsymbol{v}_1$. The dashed line is the first principal component. (c) Direction of attention. The solid arrow is the repulsive force $\boldsymbol{r}$. The dashed arrow is the forward direction of the robot $\boldsymbol{w} = (0,1)^\top$. The bold arrow is the control force $\boldsymbol{p}$. Since the obstacle is at the upper right of the image, the repulsive force $\boldsymbol{v}_1$ is towards the lower left.

Repulsive Force by Principal Component Analysis Setting $\mathbf{G} = \{\boldsymbol{g}_i\}_{i=1}^N$ to be the collection of the gradient vectors in the x-y coordinate system, we compute the principal direction of vectors in the vector set $\mathbf{G}$. An example of the collection of gradient vectors $\mathbf{G}$ is plotted in Fig. 6(a). Using the centroid $\overline{\boldsymbol{g}} = \frac{1}{N}\sum_{i=1}^N \boldsymbol{g}_i$ of $\mathbf{G}$, we define matrix $\boldsymbol{G} = (\boldsymbol{h}_1, \boldsymbol{h}_2, \cdots, \boldsymbol{h}_N)$ for $\boldsymbol{h}_i = \boldsymbol{g}_i - \overline{\boldsymbol{g}}$. Then, the 2×2 matrix

$$\boldsymbol{M} = \frac{1}{N}\boldsymbol{G}\boldsymbol{G}^\top \tag{7}$$

is the correlation matrix of vectors in $\mathbf{G}$. For eigenvalues λ_i for $i = 1, 2$ such that $\lambda_1 \geq \lambda_2$ of matrix $\boldsymbol{M}$, we set the corresponding principal components as $\boldsymbol{v}_1$ and $\boldsymbol{v}_2$, respectively. From eigenvectors $\boldsymbol{v}_1$ and $\boldsymbol{v}_2$ of matrix $\boldsymbol{M}$, we compute the direction of the attractive force to avoid colliding with the obstacles, since potential is computed from the binary function whose value is one in the obstacle area. Figure 6(b) shows an example of the first principal component of $\mathbf{G}$.

Since the robot is required to avoid collision with obstacles, the direction of the repulsive force is from the obstacle region to the dominant plane. Therefore, we define the direction of the repulsive force from obstacles as

$$\boldsymbol{r} = arg\{\min \angle[\overline{\boldsymbol{g}}, \boldsymbol{v}_1]\}, \tag{8}$$

where $\angle[\boldsymbol{a}, \boldsymbol{b}]$ is the smaller angle between vectors $\boldsymbol{a}$ and $\boldsymbol{b}$. That is, we select the direction of the mean value $\overline{\boldsymbol{g}}$ in the principal component $\boldsymbol{v}_1$ as the direction of the repulsive force from obstacles. The geometrical relationship between the principal component $\boldsymbol{v}_1$ and the repulsive force $\boldsymbol{r}$ is shown in Fig. 5 (d).

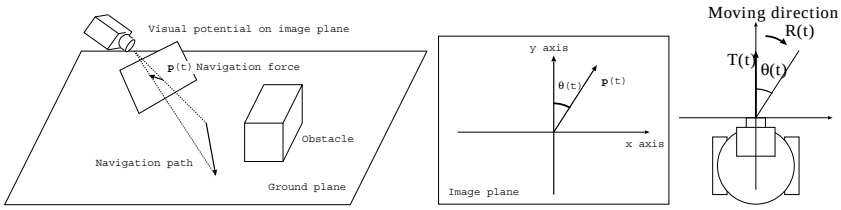

(a) (b) (c)

Fig. 7. Navigation from potential field. (a) Navigation force $\boldsymbol{p}(t)$ is the local navigation path. (b) The angle between the control force $\boldsymbol{p}(t)$ and y axis is $\theta(t)$. (c) Robot displacement $T(t)$ and rotation angle $R(t)$ at time t are determined using $\theta(t)$.

Mobile Robot Navigation by PCA Since the vector $\boldsymbol{r}$ defines the navigation direction for avoiding collision with obstacles, we set the control force as

$$\boldsymbol{p} = \boldsymbol{r} + \boldsymbol{w} \tag{9}$$

for guiding force $\boldsymbol{w}$ computed from the translational optical flow field. This direction $\boldsymbol{p}$ defines the direction of attention for the next view.

Setting $\boldsymbol{p}(t)$ to be the control force $\boldsymbol{p}$ at time t, we define the translational and rotational velocities for a nonholonomic mobile robot. We set

$$\theta(t) = \arccos \frac{\boldsymbol{p}(t)^\top \boldsymbol{y}}{|\boldsymbol{p}||\boldsymbol{y}|}, \tag{10}$$

where $\boldsymbol{y} = (0,1)^\top$ is the y axis of the image, which is the forward direction of the mobile robot. In Fig. 7, (a) and (b) show the relationships among $\boldsymbol{p}(t)$, $\theta(t)$ and the direction of robot motion [13], respectively.

We define the robot translational velocity $T(t)$ and the rotational velocity $R(t)$ at time t as $T(t) = T_m \cos\theta(t)$ and $R(t) = R_m \sin\theta(t)$, where T_m and R_m are the maximum translational and rotational velocities of the mobile robot between time t and $t+1$. Setting $\boldsymbol{X}(t) = (X(t), Y(t))^\top$ to be the position of the robot at time t in the world coordinate system, we have the relations $\sqrt{\dot{X}(t)^2 + \dot{Y}(t)^2} = T(t)$ and $\tan^{-1}\frac{\dot{Y}(t)}{\dot{X}(t)} = R(t)$. Therefore, we have the control law $\dot{X}(t) = T(t)\cos R(t)$ and $\dot{Y}(t) = T(t)\sin R(t)$ as shown in Fig. 7 (c). The control strategy is illustrated in Figure 7.

4 Experimental Results

For the computation of optical flow, we set the number of layers K as 3 for the Lucas-Kanade method with pyramids.

The mobile robot moves on the dominant plane toward the obstacle. The captured image sequence and computed optical flow $\boldsymbol{u}(t)$ are shown in the first

and second rows in Fig. 8, respectively. The optical flow $\boldsymbol{u}(t)$ and supervisor signal $\hat{\boldsymbol{u}}$ are used as a pair of input signals to fast ICA. We use the *Fast ICA package for MATLAB* [9] for the computation. The result of ICA is shown in the third row in Fig.8.

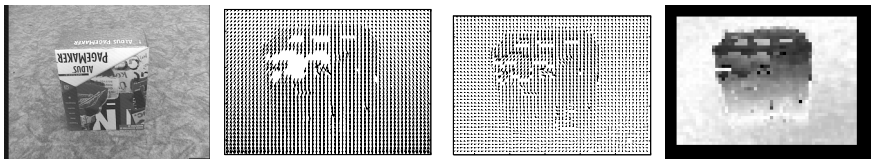

Fig. 8. From left to right, observed image $I(x, y, t)$, computed optical flow $\boldsymbol{u}(t)$, output signal $\boldsymbol{v}(t)$, and image of the dominant plane $D(x, y, t)$, respectively. In the image of the dominant plane, the white areas are the dominant planes and the black areas are the obstacle areas.

We carried out experiments on navigating the mobile robot using the proposed algorithm in real environments. The name of the mobile robot is Magellan Pro, AAI Systems, Inc. The specifications of the mobile robot are an AMD-K6 processor of 800MHz and a 256MB main memory. The environments for the experiments are counterclockwise- and clockwise-curved pathways. In these environments, the robot moved without colliding with obstacles in the corridor.

The experimental results in the counterclockwise- and clockwise-curved pathways are shown in Figs. 9 and 10, respectively. In these figures, starting from the upper left, the snapshot of the experiment, captured image $I(x, y, t)$, detected dominant plane $d(x, y, t)$, Gaussian image $G * d(x, y, t)$, gradient vector field $\boldsymbol{g}(x, y, t) = \nabla(G * d(x, y, t))$, plotted gradient vectors $\mathbf{G}$ and its first principal component $\boldsymbol{v}_1$, and direction of attention $\boldsymbol{p}$ at a frame are shown.

Figure 9 shows that the robot moved along the counterclockwise-curved pathway without colliding with obstacles. Since the obstacle is at the upper right in the image, the direction of attention is towards the upper left. Figure 9 shows that the robot moved along the clockwise-curved pathway without collision with obstacles. Since the obstacle is at the upper left in the image, the direction of attention is towards the upper right. These results show the performance of our algorithm for real environments.

5 Conclusions

We developed an algorithm for navigating a mobile robot using the independent component of the optical flow fields and the principal component of the gradient of the obstacle potential field. The ICA separates the free space and obstacle area. We defined the principal component as the repulsive force from obstacles for avoiding collision with obstacles. Our algorithm enabled a mobile robot to avoid obstacles without referring to any environmental maps. Some experimental

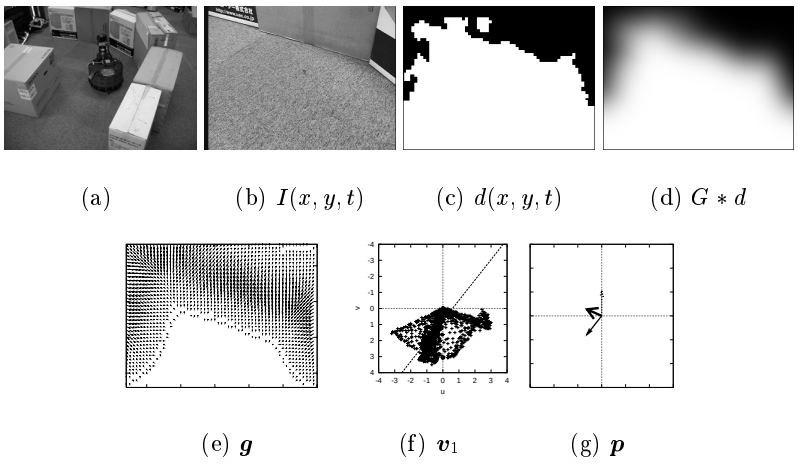

(a) (b) $I(x, y, t)$ (c) $d(x, y, t)$ (d) $G * d$

(e) $\boldsymbol{g}$ (f) $\boldsymbol{v}_1$ (g) $\boldsymbol{p}$

Fig. 9. Experimental results for the counterclockwise curved pathway. (a) Snapshot of the experiment. (b) Captured image $I(x, y, t)$. (c) Detected dominant plane $d(x, y, t)$. (d) Gaussian image $G * d(x, y, t)$. (e) Gradient vector field $\boldsymbol{g}(x, y, t) = \nabla(G * d(x, y, t))$. (f) Plotted gradient vectors $\mathbf{G}$ and its first principal component $\boldsymbol{v}_1$. (e) Direction of attention $\boldsymbol{p}$. Since the obstacle is at the upper right in the image, the direction of attention is towards the upper left.

results for a mobile robot navigating in synthetic and real environments were presented.

References

1. Adorini, G., Cagnoni, S., Mordonini, M., and Sgorbissa, A.: Omnidirectional stereo systems for robot navigation. OMNIVIS03, (2003)
2. Bouguet, J.-Y.: Pyramidal implementation of the Lucas Kanade feature tracker description of the algorithm. Intel Corporation, Microprocessor Research Labs, OpenCV Documents, (1999)
3. Conner, D. C., Rizzi, A. A., and Choset, H.: Composition of local potential functions for global robot control and navigation. International Conference on Intelligent Robots and Systems, **4** (2003) 3546–3551
4. Fermüller, C., Shulman, D, and Aloimonos, Y.: The statistics of optical flow. CVIU, **82** (2001) 1–32
5. Hyvarinen, A. and Oja, E.: Independent component analysis: algorithms and application. Neural Networks, **13** (2008) 411-430
6. Fischler, M. A. and Bolles, R. C.: Random sample consensus: A paradigm for model fitting with applications to image analysis and automated cartography. Comm. of the ACM, **24** (1981) 381–395
7. Guilherme, N. D. and Avinash, C. K.: Vision for mobile robot navigation: A survey. IEEE Trans. on PAMI, **24** (2002) 237–267
8. Horn, B. K. P. and Schunck, B. G.: Determining optical flow. Artificial Intelligence, **17** (1981) 185–203

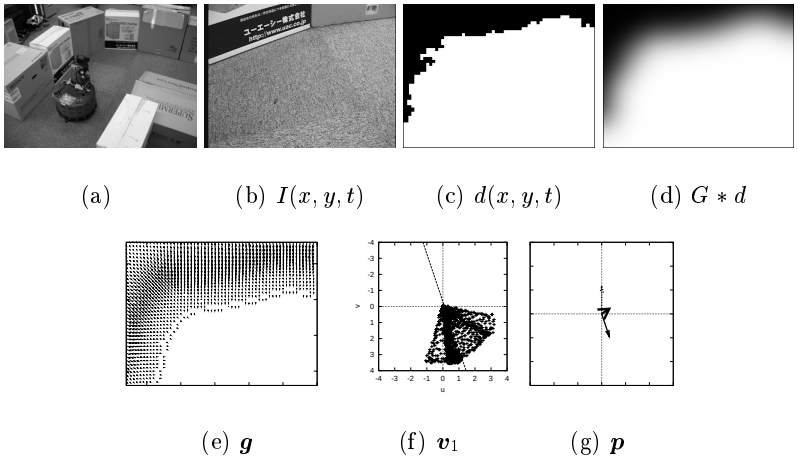

(a) (b) $I(x, y, t)$ (c) $d(x, y, t)$ (d) $G * d$

(e) $\boldsymbol{g}$ (f) $\boldsymbol{v}_1$ (g) $\boldsymbol{p}$

Fig. 10. Experimental results for the clockwise curved pathway. Captions of (a)-(e) are the same as those of Fig. 9. Since the obstacle is at the upper left in the image, the direction of attention is towards the upper right.

9. Hurri, J., Gavert, H., Sarela, J., and Hyvarinen, A.: The FastICA package for MATLAB, website: http://www.cis.hut.fi/projects/ica/fastica/
10. Khatib, O.: Real-time obstacle avoidance for manipulators and mobile robots. International J. of Robotics Research, **5** (1986) 90–98
11. Murray, D. and Little, J.: Using real-time stereo vision for mobile robot navigation. Autonomous Robots, **8** (2000) 161–171
12. Ohnishi, N. and Imiya, A.: Dominant plane detection from optical flow for robot navigation. Pattern Recognition Letters, **27** (2006) 1009–1021
13. Ohnishi, N. and Imiya, A.: Navigation of nonholonomic mobile robot using visual potential field. International Conference on Computer Vision Systems, (2007)
14. Ohnishi, N. and Imiya, A.: Independent component analysis of layer optical flow and its application. 2nd International Symposium on Brain, Vision and Artificial Intelligence, (2007) 171–180
15. Ohnishi, N. and Imiya, A.: Independent component analysis of optical flow for robot navigation. Neurocomputing, **71** (2008) 2140-2163
16. Park, K.-Y., Jabri, M., Lee, S.-Y., and Sejnowski, T. J.: Independent components of optical flows have MSTd-like receptive fields, Proc. of the 2nd International Workshop on ICA and Blind Signal Separation. (2000) 597–601
17. Roth, S. and Black, M. J.: On the spatial statistics of optical flow. IEEE International Conference on Computer Vision, **1** (2005) 42–49.
18. Wong, B. and Spetsakis, M.: Scene reconstruction and robot navigation using dynamic fields. Autonomous Robots, **8**, (2000) 71–86
19. Zemel, R. S. and Sejnowski, T. J.: A model for encoding multiple object motions and self-motion in area mst of primate visual cortex. Neuroscience, **18** (1998) 531–547